


# $\beta$ -Carotene conversion to vitamin A delays atherosclerosis progression by decreasing hepatic lipid secretion in mice

Felix Zhou<sup>1,†</sup>, Xiaoyun Wu<sup>2,†</sup>, Ivan Pinos<sup>2,3</sup>, Benjamin M. Abraham<sup>2</sup>, Tessa J. Barrett<sup>1</sup>, Johannes von Lintig<sup>4</sup> , Edward A. Fisher<sup>1</sup>, and Jaume Amengual<sup>2,3,\*</sup> 

<sup>1</sup>Cardiovascular Research Center, Leon H. Charney Division of Cardiology, Department of Medicine, New York University Grossman School of Medicine, New York, NY, USA; <sup>2</sup>Department of Food Science and Human Nutrition, University of Illinois Urbana Champaign, Urbana, IL, USA; <sup>3</sup>Division of Nutritional Sciences, University of Illinois Urbana Champaign, Urbana, IL, USA; and <sup>4</sup>Department of Pharmacology, School of Medicine, Case Western Reserve University, Cleveland, OH, USA

**Abstract** Atherosclerosis is characterized by the pathological accumulation of cholesterol-laden macrophages in the arterial wall. Atherosclerosis is also the main underlying cause of CVDs, and its development is largely driven by elevated plasma cholesterol. Strong epidemiological data find an inverse association between plasma  $\beta$ -carotene with atherosclerosis, and we recently showed that  $\beta$ -carotene oxygenase 1 (BCO1) activity, responsible for  $\beta$ -carotene cleavage to vitamin A, is associated with reduced plasma cholesterol in humans and mice. In this study, we explore whether intact  $\beta$ -carotene or vitamin A affects atherosclerosis progression in the atheroprone LDLR-deficient mice. Compared with control-fed *Ldlr*<sup>-/-</sup> mice,  $\beta$ -carotene-supplemented mice showed reduced atherosclerotic lesion size at the level of the aortic root and reduced plasma cholesterol levels. These changes were absent in *Ldlr*<sup>-/-</sup>/*Bco1*<sup>-/-</sup> mice despite accumulating  $\beta$ -carotene in plasma and atherosclerotic lesions. We discarded the implication of myeloid BCO1 in the development of atherosclerosis by performing bone marrow transplant experiments. Lipid production assays found that retinoic acid, the active form of vitamin A, reduced the secretion of newly synthesized triglyceride and cholesteryl ester in cell culture and mice.  Overall, our findings provide insights into the role of BCO1 activity and vitamin A in atherosclerosis progression through the regulation of hepatic lipid metabolism.

**Supplementary key words** retinoids • retinoic acid • cholesterol • very low density lipoprotein • carotenoids • foam cells • carotenoid • oxygenases • low density lipoprotein-cholesterol • liver

Carotenoids, a group of bioactive compounds present in most vegetables, are responsible for the yellow pigmentation of human plasma and atherosclerotic lesions (1).  $\beta$ -carotene is one of the most abundant dietary carotenoids, with human plasma concentrations inversely associated with a host of metabolic diseases, including obesity, non-alcoholic fatty liver disease, and atherosclerotic cardiovascular disease (ASCVD) (2–6).  $\beta$ -carotene is the primary

precursor of vitamin A and its metabolite retinoic acid, a potent nuclear receptor activator involved in the regulation of lipid metabolism and antiinflammatory macrophage polarization (7).

The  $\beta$ -carotene oxygenase 1 (BCO1) catalyzes the conversion of  $\beta$ -carotene to VA (8). Unlike humans, rodents do not accumulate  $\beta$ -carotene in tissues, which limits the feasibility of studying whether intact  $\beta$ -carotene performs a biological activity other than VA production. Several years ago we characterized BCO1-deficient mice, which overcome this limitation; when fed  $\beta$ -carotene, *Bco1*<sup>-/-</sup> mice accumulate  $\beta$ -carotene in tissues and plasma, as it occurs in humans (9).

We recently showed that, in humans and mice, increased BCO1 activity is associated with a decrease in total plasma cholesterol and the cholesterol carried by the non-HDL-C (10). However, we did not examine whether the changes in plasma cholesterol affect the development of atherosclerosis.

In this study, we crossed *Bco1*<sup>-/-</sup> mice with *Ldlr*<sup>-/-</sup> mice to examine whether intact  $\beta$ -carotene or its vitamin A metabolites affect atherosclerosis progression and, if so, the molecular mechanisms underlying these effects. Utilizing cell-culture studies and animal models, we also studied the mechanisms by which  $\beta$ -carotene and VA regulate plasma cholesterol concentration and whether the specific ablation of BCO1 in myeloid cells affects atherosclerosis development.

## MATERIALS AND METHODS

### Animals and diets

The studies were performed in compliance with the guidelines published in the National Institutes of Health's *Guide for the Care and Use of Laboratory Animals*. The Institutional Animal Care and Use Committees of the New York University School of Medicine and the University of Illinois at Urbana-Champaign reviewed and approved the protocol. In all studies, mice were from a C57BL/6 genetic background. We obtained *Ldlr*<sup>-/-</sup> mice and wild-type mice from Jackson Labs (Bar Harbor, ME). *Bco1*<sup>-/-</sup> mice were obtained from Case Western Reserve University (9). Mice were maintained at 24°C on a 12 h light/dark cycle and had free access

This article contains [supplemental data](#).

<sup>†</sup>These authors contributed equally to the work.

\*For correspondence: Jaume Amengual, jaume6@illinois.edu.



to food and water. We fed dams and pups a nonpurified diet containing 15 IU VA/g (Teklad global 18% protein diet; Envigo, Indianapolis, IN). Pups were weaned at 3 weeks of age. For the dietary interventions, mice were weaned onto the same diet for another week before being switched to a VA-deficient (VAD) WD containing 0.3% cholesterol, WD- $\beta$ -carotene, or WD providing 4 IU retinyl acetate/g (WD-VA).  $\beta$ -Carotene was incorporated in the diet using a water-soluble formulation of beadlets (DSM Ltd., Sisseln, Switzerland) and prepared by Research Diets (New Brunswick, NJ) by cold extrusion to protect the  $\beta$ -carotene from heat. WD-VAD and WD-VA contained placebo beadlets (without  $\beta$ -carotene) and were prepared as WD- $\beta$ -carotene. The composition of the diets is described in supplemental Table S1.

Mice were anesthetized with an 80 mg ip ketamine/kg body weight injection and then euthanized. Blood was drawn directly from the heart using EDTA-coated syringes and kept on ice. Mice were then perfused with 10% sucrose in saline solution (0.9% NaCl in water) for approximately 2 min. After perfusion, organs and the aortic roots were harvested. Portions of the liver were snap-frozen in liquid nitrogen and subsequently stored at  $-80^{\circ}\text{C}$ . Aortic roots were cleaned under a magnifying lens, embedded in optimal cutting temperature (OCT) compound (Sakura, Torrance, CA), and OCT blocks were immediately frozen at  $-80^{\circ}\text{C}$ .

### HPLC analysis of carotenoids and retinoids

Nonpolar compounds were extracted from 100  $\mu\text{l}$  plasma or tissue homogenates under a dim red safety light as described previously (11, 12). For molar quantification of  $\beta$ -carotene and retinoids, the HPLC was scaled with a standard curve using the parent compound.

### Western blot analysis of murine plasma RBP4

RBP4 plasma levels were quantified as described previously (13). Briefly, samples were subjected to SDS-PAGE and then electroblotted onto a PVDF membrane. Membranes were blocked and incubated overnight with a rabbit anti-human RBP4 serum (DakoCytomation, Denmark). We visualized RBP4 using a secondary antibody conjugated to a fluorophore (Li-Cor Biosciences, Lincoln, NE). Ponceau S staining solution (Boston BioProducts, Ashland, MA) served as a loading control for albumin visualization. Scanned immunoblots were quantified with ImageJ software (14).

### Lipid and lipoprotein analysis

Plasma total cholesterol, the cholesterol carried by HDL-C, and triglyceride concentrations were measured by colorimetric assays (FUJIFILM Wako Diagnostics, Mountain View, CA) according to the manufacturer's instructions. Non-HDL-C was determined by subtracting HDL-C from the total cholesterol concentration. Plasma lipoproteins were separated using fast-performance LC with two Superose 6 10/300 GL columns (GE Healthcare, Boston, MA) on a Shimadzu HPLC system (Columbia, MD).

### Bone marrow transplant experiments

Eight-week-old male and female *Ldlr*<sup>-/-</sup>/*Bco1*<sup>-/-</sup> mice were lethally irradiated with a double dose of 550 rads (5.5 Gy) from a cesium source 4 h apart. Ten hours later, mice were transplanted with freshly isolated bone marrow from donor wild-type or *Bco1*<sup>-/-</sup> mice in sterile cell-culture growth medium containing 100 U/ml penicillin/100  $\mu\text{g}/\text{ml}$  streptomycin. Each recipient mouse was anesthetized with isoflurane and injected with approximately  $2 \times 10^6$  bone marrow cells through retro-orbital injection. For the atherosclerosis studies, 4 weeks after bone marrow transplantation, mice were fed WD- $\beta$ -carotene for 16 weeks. The mice were euthanized for analysis at the end of the 16 weeks.

### Flow cytometry

In parallel to the atherosclerosis studies, *Ldlr*<sup>-/-</sup>/*Bco1*<sup>-/-</sup> (CD45.2) recipient mice were irradiated and injected with bone marrow from CD45.1 mice (Jackson Labs) to determine bone marrow transplant efficiency. Eight weeks after transplantation, the grafting efficiency was quantified in white blood cells from freshly collected blood using CD45.1 conjugated to Alexa488 (BioLegend, San Diego, CA) and CD45.2 conjugated to Brilliant Violet 421 (BioLegend). Flow cytometry was performed on an LSR HTS (BD Biosciences), and the data were analyzed in FlowJo.

### Cell-culture experiments: steady-state labeling studies and retinoic acid treatment

McArdle RH-7777 (McA) cells obtained from the ATCC were grown in culture plates coated with type I collagen from calfskin (Sigma-Aldrich; St. Louis, MO). McA cells were cultured in DMEM supplemented with 10% FBS (Gemini; Alachua, FL), 10% horse serum (Gemini), 1% L-glutamine, and 100 U/ml penicillin/100  $\mu\text{g}/\text{ml}$  streptomycin at  $37^{\circ}\text{C}$  with 5%  $\text{CO}_2$ .

Cholesteryl ester and triglyceride labeling was performed on independent experiments using 0.1  $\mu\text{Ci}$  [ $^3\text{H}$ ]cholesterol or 0.25  $\mu\text{Ci}$  [ $^{14}\text{C}$ ]glycerol in each well for 4 h, respectively. Total lipids in the media and cell lysates were extracted using Dole's method (15) and separated on a silica gel TLC (Thermo Fisher Scientific Inc., Waltham, MA) using a mixture of hexane-diethyl ether-acetic acid (78:20:2) as a mobile phase.

apoB labeling was performed as previously described (16). Briefly, McA hepatocytes were preincubated for 2 h in amino acid-starvation DMEM without methionine-cysteine, 1% FBS, 1% L-glutamine, and penicillin-streptomycin). After preincubation, we added 120  $\mu\text{Ci}/\text{ml}$  of the  $^{35}\text{S}$  protein labeling mix (PerkinElmer, Waltham, MA) for 4 h. After incubation, conditioned media and cell lysates were used for the immunoprecipitation of labeled apoB, and quantification was performed as previously described (16). Albumin was used as a loading control.

Retinoic acid (2  $\mu\text{M}$ ) (Cayman Chemicals, Ann Arbor, MI) was dissolved in DMSO (Sigma-Aldrich). Vehicle (DMSO) in control wells was added to a maximum volume of 0.1% in treatment media.

### Determination of triglyceride, cholesterol, and apoB100 secretion rates in mice

After an overnight fasting period, 6-week old wild-type mice fed a standard chow diet were given an intraperitoneal injection of retinoic acid dissolved in DMSO and emulsified in PBS (1:10) or vehicle (DMSO + PBS). The dose, 30 mg retinoic acid/kg body weight, was selected on the basis of previous publications (11, 17–20). The maximum injection volume was 150  $\mu\text{l}$ . Two hours later, we added 200  $\mu\text{Ci}$  of the  $^{35}\text{S}$  protein labeling mix (PerkinElmer) combined with 1,000 mg/kg pluronic F127 poloxamer-407 (Sigma-Aldrich) to inhibit lipoprotein clearance from plasma, as described previously (16). Blood samples were collected every hour from the tail to determine the secretion rate of triglyceride and total cholesterol using commercially available kits (FUJIFILM Wako Diagnostics, Mountain View, CA). apoB secretion rates were quantified by subjecting 1  $\mu\text{l}$  plasma to 8% SDS-PAGE. Gels were fixed, dried, and imaged using the Typhoon Trio laser scanner (GE Healthcare). Gel loading was normalized to total labeled protein obtained after precipitation with the trichloroacetic acid method. Secretion rate data are represented as the average result for each time point and as the average of the slope.

### Aortic root analysis

Aortic roots were removed after perfusion with 10% sucrose/saline, embedded in OCT, and frozen at  $-80^{\circ}\text{C}$ . Serial sections of

6  $\mu\text{m}$  thickness were cut and stained for CD68 (AbD Serotec, Oxford, UK) and hematoxylin/eosin, as described previously (21), or neutral lipids using Oil Red O (ORO) (Sigma-Aldrich). ImagePro Plus 7.0 (Media Cybernetics, Rockville, MD) was used with bright-field images of CD68-stained slides at 10 $\times$  magnification to determine the percentage of CD68<sup>+</sup> staining in the atherosclerotic lesion. Cholesterol crystal images were acquired using an Axioscan microscope (Carl Zeiss, Jena, Germany) using a 10 $\times$  air objective. Cholesterol crystal images were captured using polarized light and represented as the percentage of plaque area as previously described (22). Nuclear staining with DAPI (Sigma-Aldrich) was used as a counterstain.

### Laser-capture microdissection and RNA sequencing

CD68<sup>+</sup> cells were isolated from atherosclerotic lesions using laser-capture microdissection as described previously (21). Briefly, we collected sections of the aortic root on polyethylene naphthalate membrane slides (Life Technologies, Carlsbad, CA), and CD68<sup>+</sup> cells from each animal were pooled. RNA was isolated and purified using the PicoPure Kit (Thermo Fisher Scientific) treated with DNase. The quality and quantity were determined using an Agilent 2100 Bioanalyzer (Agilent Technologies, Santa Clara, CA). RNA samples with an RNA integrity number above six were amplified using the Automated Nugen Ovation Trio Low Input RNA kit (Nugen, Manchester, UK). Samples were sequenced using the HiSeq 4000 Paired-End (Illumina, San Diego, CA), and the results were analyzed using gene set enrichment analysis (Broad Institute Inc., Cambridge, MA).

### RNA sequencing data analysis

Sequencing reads were mapped to the reference genome (mm10) using STAR aligner version 2.5.0c (23). Alignments were guided by a gene transfer format file. The mean read insert sizes and their standard deviations were calculated using Picard tools (version 1.126). The read count tables were generated using HTSeq version 0.6.0 (24) and normalized on the basis of their library size factors using DESeq2 (25), and differential expression analysis was performed. The read per million normalized BigWig files were generated using BEDTools version 2.17.0 (26) and bedGraphToBigWig version 4. To compare the level of similarity among the samples and their replicates, we used two methods: principal-component analysis and Euclidean distance-based sample clustering. All downstream statistical analyses and generating plots were performed in R version 3.1.1.

### Real-time PCR analyses

Quantitative real-time PCRs of liver and intestine were performed using TaqMan Fast Advanced Master Mix (Applied Biosystems, Foster City, CA) and the following primers (Integrated DNA Technologies, Coralville, IA) and probes (Applied Biosystems): mouse intestine-specific homeobox (*Isx*; 5'-ATCTGGCTT-GTCCTTCTCC-3' and 5'-TTTTCTCTTCTGGGGCTGA-3'), mouse tubulin (5'-CAGGGCTTCTGGTTTCC-3' and 5'-GGTG-GTGTGGGTGGTGAG-3'), mouse scavenger receptor class B type 1 (Sr-bI, Mm00450234\_m1), mouse cytochrome P450 26a1 (*Cyp26a1*, Mm00514486\_m1), mouse apoC-III (*apoC-III*, Mm00445670\_m1), mouse microsomal triglyceride transfer protein (*Mttp*, Mm00435015\_m1), mouse *apoB* (Mm01545150\_m1), mouse lecithin-retinol-acyltransferase (*Lrat*; 5'-GGAACAAGTGC-GAACACTTTG-3' and 5'-CCAGACATCATCCACAAGCA-3'), rat *Cyp26a1* (Rn00590308\_m1), rat tubulin (Rn01431594\_m1), rat *apoC-III* (Rn00560743\_g1), rat *Mttp* (Rn01522963\_m1), and rat *apoB* (Rn01499054\_m1). Gene expression analyses were performed with the StepOnePlus Real-Time PCR System (Applied

Biosystems) and the  $\Delta\Delta\text{Ct}$  calculation method using tubulin as housekeeping gene.

### Cholesterol absorption dual-isotope method

Four-week-old *Ldlr*<sup>-/-</sup> mice were fed either WD-VAD or WD-VA for 12 weeks prior to quantifying cholesterol absorption by the fecal dual-isotope method (27). At the end of this intervention, mice were gavaged 200  $\mu\text{l}$  olive oil containing 1  $\mu\text{Ci}$  [<sup>14</sup>C]cholesterol (American Radiolabeled Chemicals, St. Louis, MO) and 2  $\mu\text{Ci}$  [<sup>3</sup>H]sitostanol (American Radiolabeled Chemicals). We estimated cholesterol uptake by either pooling all of the feces at the end of 4 days ( $n = 5$  mice/group) or by collecting the feces every 24 h during 4 consecutive days ( $n = 4$  mice/group).

In both experiments, feces were dried using a SpeedVac vacuum concentrator (Eppendorf, Hamburg, Germany) and ground into powder. We weighted approximately 100 mg feces per sample and dissolved them overnight with 1.5 ml distilled water. Samples were saponified in 3 ml ethanol, 300  $\mu\text{l}$  12% pyrogallol (Sigma-Aldrich) in ethanol, and 600  $\mu\text{l}$  30% potassium hydroxide in water at 37°C for 2 h. The total lipid content was extracted twice with a mixture of diethylether:hexane:ethanol (66:33:1). The supernatants of all samples were collected and evaporated in a SpeedVac and resuspended in scintillation liquid cocktail (PerkinElmer). [<sup>14</sup>C]cholesterol and [<sup>3</sup>H]sitostanol were measured with an LS6500 scintillation counter (Beckman, Brea, CA). The calculation of the percentage of cholesterol absorption followed Wang and Carey's methodology (27).

### Statistical analyses

Data are expressed as means  $\pm$  SEMs. Statistical differences were analyzed using GraphPad Prism software (GraphPad Software Inc., San Diego, CA). The normal distribution of the sample groups was analyzed using the D'Agostino-Pearson omnibus and Shapiro-Wilk normality tests. Data were analyzed either using two-way ANOVA (GraphPad Prism) with Dunnett's multiple comparison testing or repeated-measures two-way ANOVA with Sidak's multiple comparisons test. Statistical significance was set at  $P < 0.05$ .

Multivariate ANOVA was performed to analyze the differences in plaque area and total cholesterol levels in mice fed WD-VAD or WD- $\beta$ -carotene simultaneously, followed by univariate one-way ANOVA to test individually each dependent variable (R Studio software version 3.6.2).

For the RNA sequencing data, we used the false-discovery rate approach to reduce the number of false positives in multiple testing. Statistical significance was set at  $P < 0.05$ .

## RESULTS

### Effects of $\beta$ -carotene supplementation on $\beta$ -carotene and retinoid levels in *Ldlr*<sup>-/-</sup> and *Ldlr*<sup>-/-</sup>/*Bco1*<sup>-/-</sup> mice

Unlike rodents, humans accumulate  $\beta$ -carotene in tissues, plasma, and atherosclerotic lesions (1). To model the human accumulation of  $\beta$ -carotene and to understand the role of  $\beta$ -carotene in the development of atherosclerosis, we generated an atherogenic mouse model (*Ldlr*<sup>-/-</sup>) capable of accumulating  $\beta$ -carotene (*Bco1*<sup>-/-</sup>). *Ldlr*<sup>-/-</sup>/*Bco1*<sup>-/-</sup> mice were born at the expected Mendelian ratio and did not show any detectable morphological or behavioral abnormalities (data not shown). To assess the effect of  $\beta$ -carotene to lesion progression, *Ldlr*<sup>-/-</sup> and *Ldlr*<sup>-/-</sup>/*Bco1*<sup>-/-</sup> mice were fed WD-VAD or WD- $\beta$ -carotene for 12 weeks

(Fig. 1A). En face visualization of the aortic arch showed that *Ldlr*<sup>-/-</sup>/*Bco1*<sup>-/-</sup> mice fed WD-β-carotene accumulate β-carotene, in line with the accumulation of β-carotene in human atherosclerotic lesions (1) (Fig. 1B). HPLC quantification confirmed this finding and showed a 10-fold higher β-carotene content in the aortic arch than the *Ldlr*<sup>-/-</sup> mice fed the same diet (Fig. 1C).

No significant changes between groups were observed in systemic vitamin A levels (all-*trans* retinol) or the vitamin A carrier RBP4 (Fig. 1D, E). Plasma β-carotene was approximately 100-fold higher in *Ldlr*<sup>-/-</sup>/*Bco1*<sup>-/-</sup> mice fed WD-β-carotene than in *Ldlr*<sup>-/-</sup> mice fed the same diet (Fig. 1F). We next quantified hepatic retinyl esters, the main vitamin A reservoir in the body (6, 28). Hepatic retinyl ester stores showed a trend toward increasing in *Ldlr*<sup>-/-</sup> mice fed WD-β-carotene compared with *Ldlr*<sup>-/-</sup> mice fed WD-VAD (Fig. 1G). This trend was accompanied by the increased expression of the retinoic acid target gene *Cyp26a1* (Fig. 1H), a surrogate marker of vitamin A status (29). We did not observe significant differences between *Ldlr*<sup>-/-</sup> mice fed WD-VAD and *Ldlr*<sup>-/-</sup>/*Bco1*<sup>-/-</sup> mice fed either WD-VAD or WD-β-carotene in either hepatic retinyl esters or hepatic

*Cyp26a1* expression (Fig. 1G, H). On the contrary, *Ldlr*<sup>-/-</sup>/*Bco1*<sup>-/-</sup> mice fed WD-β-carotene presented approximately a 6-fold increase in β-carotene stores compared with *Ldlr*<sup>-/-</sup> mice fed the same diet (Fig. 1I). Together, these results show that β-carotene was converted to vitamin A in *Ldlr*<sup>-/-</sup> mice but not in *Ldlr*<sup>-/-</sup>/*Bco1*<sup>-/-</sup> mice, although none of the experimental groups suffered from systemic or hepatic vitamin A deficiency during the dietary intervention.

### β-Carotene supplementation delays atherosclerosis progression in *Ldlr*<sup>-/-</sup> mice but not in *Ldlr*<sup>-/-</sup>/*Bco1*<sup>-/-</sup> mice

Next, we analyzed plasma cholesterol partitioning in pooled samples (*n* = 5 mice/group) by fast-performance LC. *Ldlr*<sup>-/-</sup> mice fed WD-β-carotene showed a decrease in the amount of VLDL-C and LDL-C compared with those fed WD-VAD. We did not observe differences in HDL-C concentrations (Fig. 2A). The presence of dietary β-carotene, however, did not affect plasma cholesterol distribution in *Ldlr*<sup>-/-</sup>/*Bco1*<sup>-/-</sup> mice (Fig. 2B). We confirmed these results in the entire mouse cohort (*n* = 9–12 mice/group) by

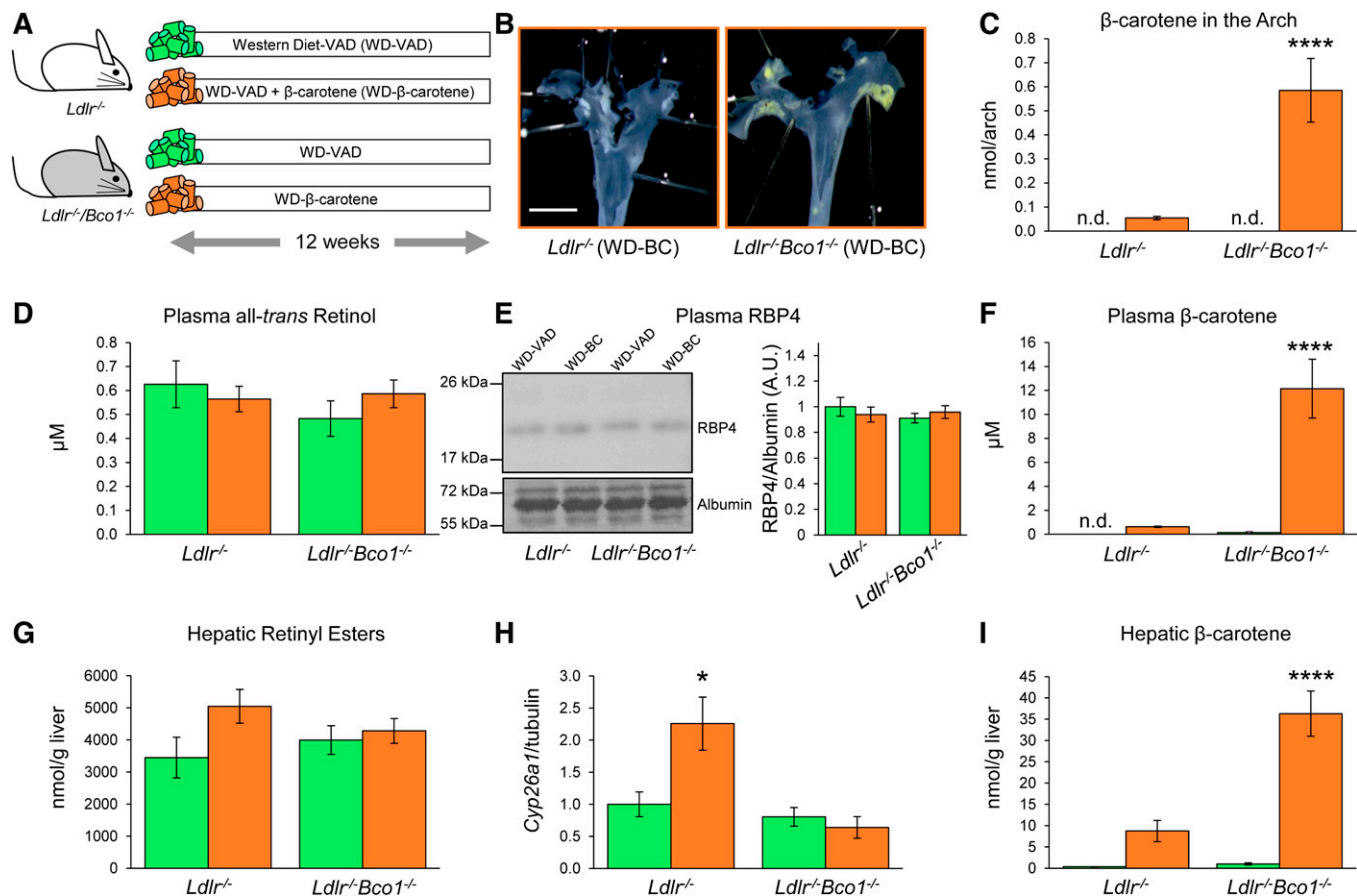


**Fig. 1.** Effects of β-carotene dietary supplementation on β-carotene and vitamin A levels in *Ldlr*<sup>-/-</sup> and *Ldlr*<sup>-/-</sup>/*Bco1*<sup>-/-</sup> mice. A: Experimental design. For 12 weeks, 4-week-old male and female *Ldlr*<sup>-/-</sup> and *Ldlr*<sup>-/-</sup>/*Bco1*<sup>-/-</sup> mice were fed WD-VAD or WD-β-carotene. B: En face visualization of atherosclerotic lesions in the aortic arch of *Ldlr*<sup>-/-</sup> and *Ldlr*<sup>-/-</sup>/*Bco1*<sup>-/-</sup> fed WD-β-carotene. C: HPLC quantification of β-carotene in the aortic arch. D, E: All-*trans* retinol in plasma and its carrier RBP4 quantified by HPLC and Western blot, respectively. F: HPLC quantification of plasma β-carotene. G: Hepatic retinyl ester stores. H: Hepatic mRNA expression of *Cyp26a1*. I: β-carotene hepatic stores. Values are represented as means ± SEMs (*n* = 9–12 mice/group). Statistical differences were evaluated using two-way ANOVA (*P* < 0.05). \*\*\*\**P* < 0.0001 considering *Ldlr*<sup>-/-</sup> WD-VAD-fed mice as a reference group. Size bar = 2 mm.

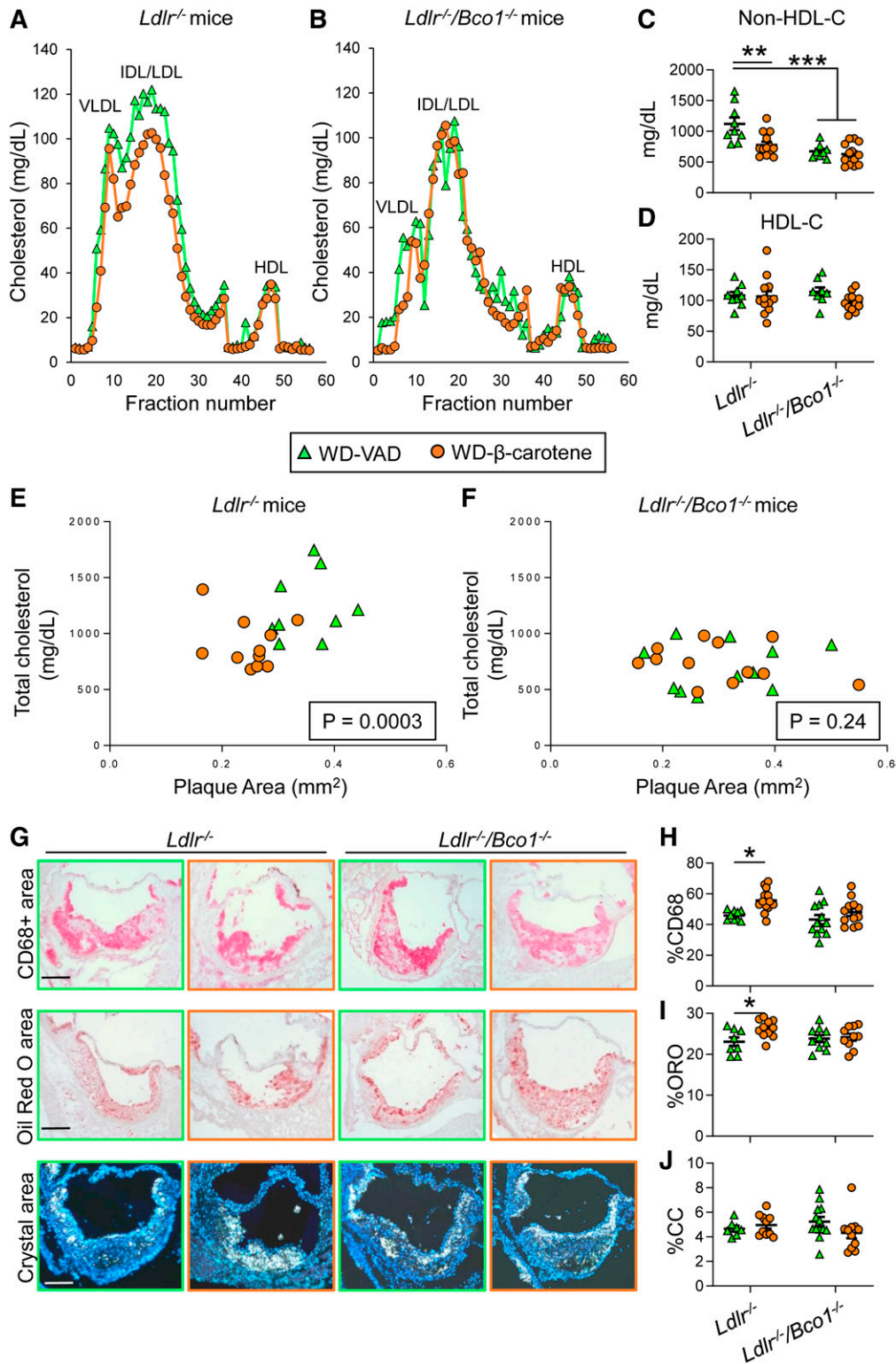


**Fig. 2.** Effects of β-carotene dietary supplementation on atherosclerosis progression in *Ldlr*<sup>-/-</sup> and *Ldlr*<sup>-/-</sup>/*Bco1*<sup>-/-</sup> mice. For 12 weeks, 4-week-old male and female *Ldlr*<sup>-/-</sup> and *Ldlr*<sup>-/-</sup>/*Bco1*<sup>-/-</sup> mice were fed WD-VAD or WD-β-carotene. A, B: Lipoprotein profiles from *Ldlr*<sup>-/-</sup> and *Ldlr*<sup>-/-</sup>/*Bco1*<sup>-/-</sup> mice fed WD-VAD or WD-β-carotene (data pooled from 5 mice/group). C, D: Non-HDL-C and HDL-C levels, respectively. E, F: Correlation between total plaque area and total cholesterol plasma levels in *Ldlr*<sup>-/-</sup> and *Ldlr*<sup>-/-</sup>/*Bco1*<sup>-/-</sup> mice fed WD-VAD and WD-β-carotene. (G) Representative images and quantifications for the relative (H) macrophage (CD68<sup>+</sup> area; red), (I) lipid (ORO; red), and (J) cholesterol crystal (CC; white) area content. Values are represented as means ± SEMs (*n* = 9–12 mice/group). Statistical differences were evaluated using two-way ANOVA (*P* < 0.05). \**P* < 0.05, \*\**P* < 0.01, and \*\*\**P* < 0.005 considering *Ldlr*<sup>-/-</sup> WD-VAD-fed mice as a reference group. Correlation between total cholesterol and plaque area was determined using multivariate ANOVA. Size bar = 200 μm.

measuring non-HDL-C and HDL-C concentrations. *Ldlr*<sup>-/-</sup> mice fed WD-β-carotene showed 30% lower non-HDL-C levels than WD-VAD-fed mice. *Ldlr*<sup>-/-</sup>/*Bco1*<sup>-/-</sup> mice did not show differences between groups, although non-HDL-C concentrations were lower than *Ldlr*<sup>-/-</sup> mice fed WD-VAD (Fig. 2C). We did not observe changes in HDL-C between genotypes or diets (Fig. 2D).

Next, we quantified total plasma cholesterol concentrations and the atherosclerotic lesion areas (plaque area) at the level of the aortic root. In *Ldlr*<sup>-/-</sup> mice, WD-β-carotene reduced total plasma cholesterol (WD-VAD = 1,229 ± 101.5 mg/dl; WD-β-carotene = 892.2 ± 62.6 mg/dl; *P* = 0.008) and total plaque area (WD-VAD = 0.351 ± 0.018 mm<sup>2</sup>; WD-β-carotene = 0.249 ± 0.01 mm<sup>2</sup>; *P* = 0.0004). On the contrary, *Ldlr*<sup>-/-</sup>/*Bco1*<sup>-/-</sup> mice showed no significant differences in total plasma cholesterol (WD-VAD = 703.6 ± 63.4 mg/dl; WD-β-carotene = 738.9 ± 49.2 mg/dl; *P* = 0.66) and total plaque area (WD-VAD = 0.309 ± 0.03 mm<sup>2</sup>; WD-β-carotene = 0.301 ± 0.03 mm<sup>2</sup>; *P* = 0.85). To determine whether plasma cholesterol levels correlated to plaque size, we plotted these measurements for both genotypes. The reduction in total plasma cholesterol in *Ldlr*<sup>-/-</sup> mice fed WD-β-carotene correlated with a reduction in plaque size area (*P* = 0.0003) (Fig. 2E). We did not observe a correlation between plasma cholesterol and plaque size in *Ldlr*<sup>-/-</sup>/*Bco1*<sup>-/-</sup> mice fed the same dietary regimens (*P* = 0.24) (Fig. 2F). These results were comparable when we evaluated the correlation between non-HDL-C and plaque size for *Ldlr*<sup>-/-</sup> mice (*P* = 0.0005) and *Ldlr*<sup>-/-</sup>/*Bco1*<sup>-/-</sup> mice (*P* = 0.89) (data not shown).

To determine the stage of the atherosclerotic lesions, we analyzed the macrophage content in the plaques by staining the aortic roots with an antibody against CD68. Foam cell content was quantified by staining neutral lipids with ORO, and the presence of cholesterol crystals was determined by polarized light microscopy (Fig. 2G). The percentage of the lesion area positive for the macrophage marker CD68 was significantly increased in *Ldlr*<sup>-/-</sup> mice fed WD-β-carotene compared with *Ldlr*<sup>-/-</sup> mice fed WD-VAD (Fig. 2H). Neutral lipid content quantification showed the same trend as observed for CD68 content (Fig. 2I). Overall, these results indicate that the lesions present in *Ldlr*<sup>-/-</sup> mice fed WD-β-carotene are smaller and enriched in macrophages and foam cells (Fig. 2E, G–I), a characteristic feature of early, progressing plaques (30). Neither the macrophage (CD68<sup>+</sup> area) nor the neutral lipid (ORO<sup>+</sup> area) contents were altered in *Ldlr*<sup>-/-</sup>/*Bco1*<sup>-/-</sup> mice fed WD-VAD or WD-β-carotene compared with *Ldlr*<sup>-/-</sup> mice fed WD-VAD (Fig. 2H, I). Cholesterol crystal content remained unchanged among all groups (Fig. 2J).

### Vitamin A supplementation reduces plasma cholesterol independently of intestinal cholesterol absorption

In line with our recent report (10), our results show that BCO1 activity reduces plasma cholesterol concentrations (Fig. 2). To examine whether dietary vitamin A can also reduce plasma cholesterol, we compared *Ldlr*<sup>-/-</sup> mice after 12 weeks on WD-VAD, WD-β-carotene, or 4 IU/g WD-VA. Both WD-β-carotene and WD-VA favored a reduction in

plasma cholesterol, which was already significant for WD-VA after 4 weeks (Fig. 3A).

Next, we determined whether vitamin A regulates intestinal cholesterol uptake. First, we measured the levels of *Isx*, a transcription factor responsible for the intestinal regulation of SR-bI (31, 32), a multiligand receptor for cholesterol and other lipids including carotenoids (33, 34). *Isx* mRNA levels were upregulated in the duodenum of mice fed WD-VA compared with those fed WD-VAD (Fig. 3B). Accordingly, *Sr-bI* expression was suppressed in mice fed WD-VA compared with those fed WD-VAD (Fig. 3C).

To evaluate whether dietary vitamin A affects cholesterol uptake, we gavaged *Ldlr*<sup>-/-</sup> mice fed WD-VAD or WD-VA (*n* = 5 mice/group) with a single dose of [<sup>3</sup>H]sitostanol and [<sup>14</sup>C]cholesterol. Next, we collected mouse feces accumulated over 4 days and measured sitostanol and cholesterol following established protocols (27). In a second experiment (*n* = 4 mice/group), we collected the feces every day. In both experimental cohorts, excreted cholesterol remained unchanged between groups, indicating that dietary vitamin A does not affect intestinal cholesterol uptake in mice (Fig. 3D, E).

### Retinoic acid, the transcriptionally active form of vitamin A, reduces hepatic lipoprotein secretion

To determine whether vitamin A reduces plasma cholesterol concentration by regulating VLDL secretion, we used McA rat hepatocytes, a well-characterized model of VLDL assembly and secretion (16, 35). We cultured McA cells in the presence of retinoic acid, the transcriptionally active form of vitamin A. As expected, McA cells exposed to 2 μM retinoic acid for 6 h showed marked induction of *Cyp26a1* (Fig. 4A). Under these experimental conditions, we quantified the secretion of newly synthesized cholesteryl esters by adding [<sup>3</sup>H]cholesterol to the cell media for 4 h. Cells exposed to retinoic acid showed approximately 30% reduction of [<sup>3</sup>H]cholesteryl ester in the media compared with vehicle-treated cells. These changes occurred without changing the radiolabeled cellular content of [<sup>3</sup>H]cholesteryl ester (Fig. 4B). To determine whether retinoic acid also decreased hepatic triglyceride secretion, the major lipid component of VLDL (36), we exposed McA cells to retinoic acid for 2 h and [<sup>14</sup>C]glycerol for the remaining 4 h of treatment. Cells exposed to retinoic acid had 30% lower hepatic triglyceride secretion than DMSO-exposed cells. Intracellular [<sup>14</sup>C]triglyceride in lysates remained unchanged between groups (Fig. 4C).

We next analyzed apoB100 secretion, an indicator of the number of VLDL particles, in the presence of a mixture of [<sup>35</sup>S]Met/Cys for 4 h and used apoB48 and albumin as internal controls in the media (Fig. 4D) and cell lysates (Fig. 4E). McA cells exposed to retinoic acid showed a reduced apoB100 secretion without affecting the apoB100 cellular content (Fig. 4F). Retinoic acid did not significantly affect the secretion or the intracellular levels of apoB48 and albumin (Fig. 4G, H).

Next, we determined whether retinoic acid also affects hepatic lipid secretion in mice. Livers of mice exposed to retinoic acid (30 mg/kg) for 6 h showed an upregulation

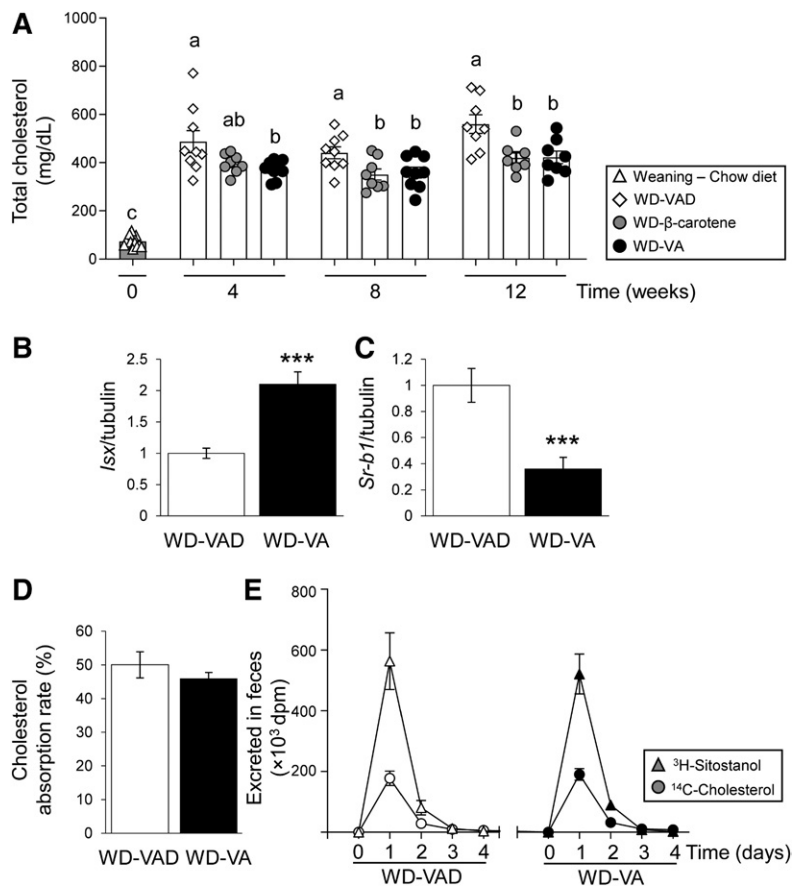


**Fig. 3.** Effect of vitamin A supplementation on intestinal cholesterol uptake. For 12 weeks, 4-week-old male and female *Ldlr*<sup>-/-</sup> mice were fed WD-VAD, WD-VA, or WD-β-carotene. **A:** Total plasma cholesterol levels measured at different time points. **B, C:** mRNA expression levels of *Isx* and *Srebp1* in the duodenum. **D, E:** Cholesterol absorption rate calculated using the fecal dual-isotope ratio method using 4-day pooled fecal samples (see Materials and Methods for details) or quantified in each individual day in two different experimental cohorts. Values are represented as means ± SEMs ( $n = 4-8$  mice/group). Statistical differences were evaluated using one-way ANOVA with Dunnett's multiple comparison testing ( $P < 0.05$ ; represented by values not sharing a common letter) or by two-tailed Student's *t*-test. \*\*\* $P < 0.005$ .

of *Cyp26a1* comparable to that shown in McA cells exposed to 2 μM retinoic acid for the same amount of time (Fig. 4A, I). Under these experimental conditions, retinoic acid-treated mice showed a reduction in cholesterol and triglyceride secretion rates compared with vehicle-treated mice (Fig. 4J, K). apoB100 secretion in vivo did not show significant changes upon retinoic acid treatment (Fig. 4L), suggesting that retinoic treatment regulated the lipid composition of VLDL particles and not the number of particles in mice.

### BCO1 myeloid-specific deletion does not affect atherosclerosis development

A previous report indicates that macrophages express BCO1, and its enzymatic activity prevents foam cell formation in cultured macrophages (37). To determine the role of BCO1 in plaque macrophages and its contribution to atherosclerosis progression and foam cell formation in vivo, we transplanted bone marrow cells from either wild-type or *Bco1*<sup>-/-</sup> donor mice into lethally irradiated *Ldlr*<sup>-/-</sup>/*Bco1*<sup>-/-</sup> mice. After a recovery period, recipient mice were fed WD-β-carotene for 16 weeks (Fig. 5A). The lack of reliable BCO1 antibodies for flow cytometry prompted us to validate bone marrow transplant efficiency in parallel experiments utilizing *Cd45.1* mice as bone marrow donors and irradiated *Ldlr*<sup>-/-</sup>/*Bco1*<sup>-/-</sup> (*Cd45.2*) recipient mice. Under our experimental conditions, we observed a transplant efficiency of greater than 98% (i.e., 98% of the myeloid cells were CD45.1<sup>+</sup>) (supplemental Fig. S1).

At the time the mice were euthanized, we did not find significant differences in total cholesterol or triglyceride plasma concentrations (supplemental Fig. S2A, B), or plasma β-carotene (supplemental Fig. S2C). To evaluate the effect of myeloid-specific BCO1 expression on plaque progression, we measured total plaque area, CD68<sup>+</sup> cell content, and ORO<sup>+</sup> area at the level of the aortic root (Fig. 5B). Findings indicated no differences between the groups, either in plaque size (Fig. 5C), CD68<sup>+</sup> area (Fig. 5D), or foam cell content (Fig. 5E). To determine whether the absence of BCO1 affects the gene expression profile in the plaque myeloid cells, we isolated CD68<sup>+</sup> cells from *Ldlr*<sup>-/-</sup>/*Bco1*<sup>-/-</sup> recipient mice transplanted with either wild-type or *Bco1*<sup>-/-</sup> bone marrow from the aortic root by laser-capture microdissection and performed RNA sequencing.

RNA sequencing data showed a total of 983 genes differentially regulated ( $P < 0.05$ ), with 386 genes upregulated and 597 genes downregulated in BCO1-deficient plaque cells compared with wild-type plaque cells (Fig. 5F, G). Consistent with the absence of BCO1, the retinoic acid target gene *Cyp26a1* was suppressed significantly in BCO1-myeloid-deficient plaque cells compared with macrophages from wild-type donors (Fig. 5H). Similarly, the aldehyde dehydrogenase 1 family member A2 (*Aldh1a2*), which is a rate-limiting enzyme in retinoic acid synthesis (38), was also downregulated in BCO1-deficient plaque cells (Fig. 5H). Gene set enrichment analysis pathway analysis showed significantly different regulation of seven distinct pathways. The TGFβ pathway was the top downregulated pathway in

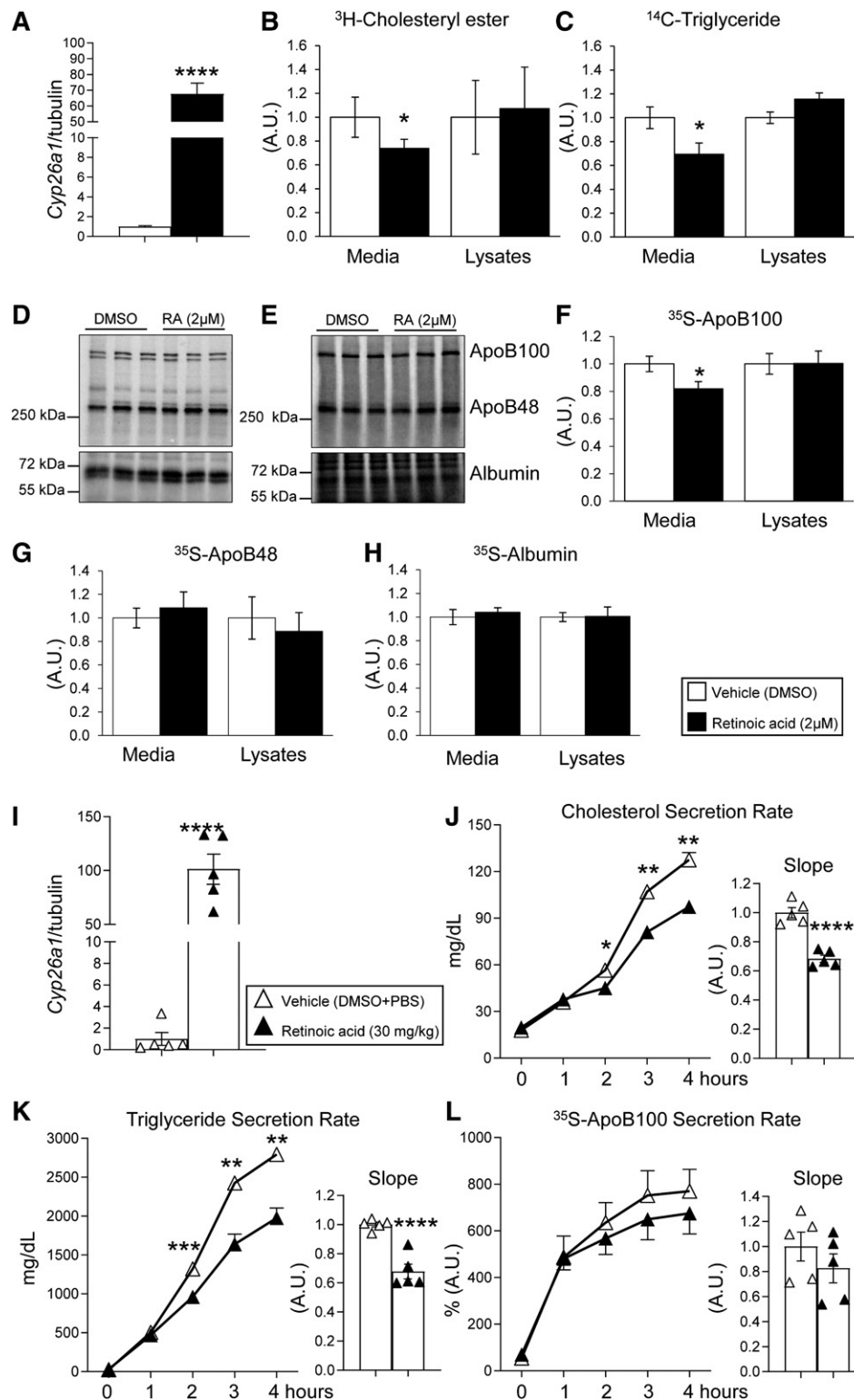


**Fig. 4.** Retinoic acid reduces apoB100 secretion in cultured hepatocytes and mice. **A:** mRNA expression of *Cyp26a1* in McA rat hepatic cells cultured in a normal growth medium and exposed to 2 μM retinoic acid or DMSO (vehicle control) for 6 h. **B, C:** McA cells exposed to 2 μM retinoic acid or DMSO (vehicle control) were subjected to steady-state metabolic labeling with either [<sup>3</sup>H]cholesterol or [<sup>14</sup>C]glycerol for the last 4 h of treatment. After incubation, cell media and lysates were collected, and radiolabeled [<sup>3</sup>H]cholesteryl esters or [<sup>14</sup>C]triglyceride were separated by TLC and quantified using a scintillation counter. **D, E:** Representative <sup>35</sup>S-radiolabeled blots of McA cells media and lysates exposed to 2 μM retinoic acid or DMSO (vehicle control) subjected to steady-state metabolic labeling with [<sup>35</sup>S]Met/Cys mixture. **F–H:** Corresponding protein quantifications for apoB100, apoB48, and albumin in the media and cell lysates. Radiolabeling experiments were performed in separate experiments in triplicate. **I:** mRNA expression of *Cyp26a1* in age and sex-matched



BCO1-deficient myeloid cells ( $P = 0.0001$ ) (Fig. 5I). BCO1-deficient plaque myeloid cells showed a downregulation of the several genes involved in the TGF $\beta$  pathway compared with wild-type cells (Fig. 5J).

The absence of BCO1 in myeloid cells did not affect systemic vitamin A status (supplemental Fig. S2D) or hepatic vitamin A or  $\beta$ -carotene levels (supplemental Fig. S2E, F). Accordingly, the expression of *Cyp26a1* and *Lrat*, two classical retinoic acid target genes in the liver (29, 39), remained unaltered between the two groups (supplemental Fig. S2G).

## DISCUSSION

We recently described an association between BCO1 activity and circulating cholesterol in mice and humans (10). In our clinical study, subjects carrying at least one copy of the *BCO1* rs6564851-T allele, which increases BCO1 activity (40), showed a reduction in total serum cholesterol and non-HDL-C concentrations. Similarly, we observed that wild-type mice fed WD- $\beta$ -carotene presented a decrease in total cholesterol and non-HDL-C concentrations compared with congenic *Bco1*<sup>-/-</sup> mice subjected to the same dietary regimen (10). These studies raised the question as to what mechanism underlies this association and whether these alterations in circulating cholesterol have a clinical significance.

Our results show that the conversion of  $\beta$ -carotene to vitamin A delays atherosclerosis progression in *Ldlr*<sup>-/-</sup> mice. Compared with *Ldlr*<sup>-/-</sup> mice fed WD-VAD, *Ldlr*<sup>-/-</sup> mice fed WD- $\beta$ -carotene presented smaller atherosclerotic plaques that were enriched with macrophages and foam cells, a characteristic feature of early-stage lesions (30). Plaque area correlated with reduced plasma cholesterol in *Ldlr*<sup>-/-</sup> mice (Fig. 2), and mice fed WD-VA showed similar results on plasma cholesterol compared with those fed WD- $\beta$ -carotene (Fig. 3A). *Ldlr*<sup>-/-</sup>/*Bco1*<sup>-/-</sup> mice fed WD  $\beta$ -carotene, which cannot convert  $\beta$ -carotene to VA, do not show significant differences either on atherosclerosis progression or plasma cholesterol compared with those fed WD-VAD (Fig. 2). We observed that *Ldlr*<sup>-/-</sup>/*Bco1*<sup>-/-</sup> mice, either fed WD-VAD or WD- $\beta$ -carotene, showed lower non-HDL-C than *Ldlr*<sup>-/-</sup> mice fed WD-VAD (Fig. 2C), suggesting that the absence of BCO1 alters cholesterol metabolism. Previous reports have shown alterations in lipid metabolism of *Bco1*<sup>-/-</sup> mice compared with wild-type controls, suggesting that BCO1 plays a direct role on lipid metabolism, one that is independent of its role in vitamin A production (9, 41, 42). Overall, this study demonstrates that the action of BCO1 and its role in vitamin A production delays atherosclerosis progression. These results paralleled those

observed with respect to obesity, in which wild-type mice fed a diet containing  $\beta$ -carotene showed a reduction in adiposity compared with those fed a control diet (43). In contrast, *Bco1*<sup>-/-</sup> mice fed the same dietary regimens did not show differences in adiposity, despite *Bco1*<sup>-/-</sup> mice accumulating large amounts of  $\beta$ -carotene in their adipose tissue (43).

Our results align with previous reports showing a reduction of plaque size in hypercholesterolemic mice fed diets fortified with either a mixture of  $\beta$ -carotene and 9-*cis*  $\beta$ -carotene, or vitamin A (44, 45). However, these authors utilized 100 times higher doses of provitamin A carotenoids than our study, while we supplemented the diet with a comparable amount of  $\beta$ -carotene found in vegetables. Regarding vitamin A, these authors utilized a diet containing over three times higher vitamin A levels than our study (45), which follows the guidelines of the American Institute of Nutrition (46). Overall, our dietary interventions confirm these previous findings on plasma cholesterol in mice, even when  $\beta$ -carotene and vitamin A are provided at physiological concentrations.

Elevated dietary cholesterol drives atherosclerosis development in *Ldlr*<sup>-/-</sup> mice (47), and it is a risk factor for the development of ASCVD in specific populations (48). Among the different molecular targets by which vitamin A could modulate intestinal cholesterol uptake, the intestine-specific transcription factor ISX caught our attention. *ISX* is a retinoic acid-responsive gene that regulates the absorption and cleavage of  $\beta$ -carotene by modulating SR-BI and BCO1 expression, respectively (32, 49). Interestingly, the binding site of ISX in the promoter region of the *BCO1* gene coincides with the *BCO1* rs6564851 allele (49). As have we described previously (10), the *BCO1* rs6564851 allele is associated with circulating cholesterol in humans. To determine whether dietary vitamin A reduces intestinal cholesterol uptake by downregulating SR-BI or via other mechanisms, we measured the cholesterol absorption rate in *Ldlr*<sup>-/-</sup> mice fed WD-VAD or WD-VA. However, our results indicate that vitamin A does not affect intestinal cholesterol uptake (Fig. 3). These data support the results of studies showing that the intestinal expression of SR-BI does not significantly alter cholesterol absorption (50). They also rule out dietary cholesterol absorption as the mechanism by which  $\beta$ -carotene and vitamin A decreased plasma cholesterol in *Ldlr*<sup>-/-</sup> mice.

Consistent with our recent publication (10), we show that the conversion of  $\beta$ -carotene to vitamin A reduces total plasma cholesterol by decreasing non-HDL-C levels (Fig. 2). Under fasting conditions, non-HDL-C consists of the cholesterol present in VLDL and its derivative LDL. The hepatic secretion of VLDL depends, at least in part, on

---

wild-type mice after receiving a single intraperitoneal injection of an emulsion containing 30 mg/kg retinoic acid dissolved in DMSO and PBS or vehicle (DMSO + PBS) for 6 h before tissue harvesting. (J) Total cholesterol, (K) triglyceride, and (L) <sup>35</sup>S-apoB100 secretion rates were determined in vivo as described in the Materials and Methods after 6 h of exposure to retinoic acid. Numerical data represent the means  $\pm$  SEMs of three independent experiments (cell cultures;  $n = 5$ –6 mice/group). Statistical differences were evaluated by unpaired Student's *t*-test or by repeated-measures two-way ANOVA. \* $P < 0.05$ , \*\* $P < 0.01$ , \*\*\* $P < 0.005$ , and \*\*\*\* $P < 0.0001$ .

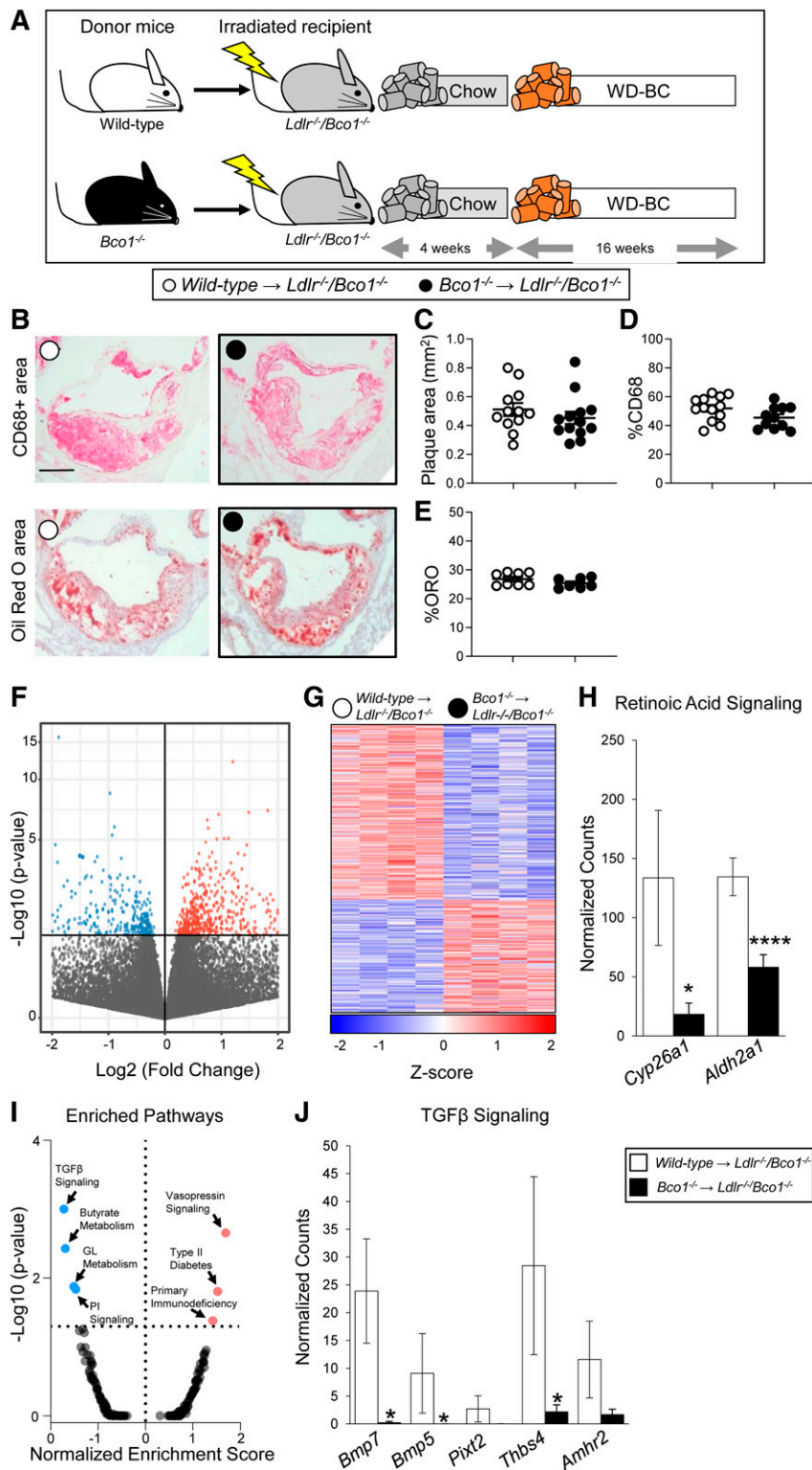


**Fig. 5.** Effects of BCO1-myeloid deficiency on plaque progression. **A:** Experimental design. Wild-type or *Bco1*<sup>-/-</sup> mice bone marrow cells were transplanted into lethally irradiated *Ldlr*<sup>-/-</sup>/*Bco1*<sup>-/-</sup> mice. After a recovery period, chimeric mice were fed WD-β-carotene for 16 weeks. **(B)** Representative images and quantifications for the **(C)** total lesion area, **(D)** macrophage (CD68% area content), and **(E)** lipid (ORO) content. **F, G:** Volcano plot and heat map showing differential gene expression between wild-type and *Bco1*<sup>-/-</sup> plaque myeloid cells. **H:** Expression levels of retinoic acid signaling genes. **I:** Volcano plot showing enriched pathway analysis. **J:** Downregulation of TGFβ pathway in *Bco1*<sup>-/-</sup> plaque cells compared with wild-type cells. Values are represented as means ± SEMs (*n* = 4–12 mice/group). Statistical differences were evaluated by unpaired Student's *t*-test. \**P* < 0.05 and \*\*\*\**P* < 0.0001. Size bar = 200 μm. GL, glycerolipid.

the intracellular apoB100 degradation rate, a complex process regulated by factors such as autophagy and endoplasmic reticulum-associated degradation (51). Our results indicate that *Ldlr*<sup>-/-</sup> mice fed WD-β-carotene have an increased retinoic acid status in hepatocytes, as shown by *Cyp26a1* hepatic expression (Fig. 1H), which results in a reduced non-HDL-C plasma levels compared with *Ldlr*<sup>-/-</sup> mice fed WD-VAD (Fig. 2A, C). These results are in agreement with the effects that direct retinoic acid exposure has on the reduction of hepatic lipid secretion (Fig. 4). These results align with the role of retinoic acid and carotenoids in obesity and ASCVD (7, 52), including fatty acid oxidation in hepatocytes and other cell types (53–57). Most of the effects of retinoic acid are derived from its role as a nuclear receptor activator, which could explain our results on hepatic lipoprotein secretion (Fig. 4). apoB is the main protein component of VLDL (51); hence, we quantified *apoB* expression in our cell culture and animal models. We did not observe any alteration upon retinoic acid exposure (supplemental Fig. S3). Next, we measured the expression of *Mtth*, which transfers triglyceride and cholesteryl esters to nascent VLDL (58). Costabile et al. (59) showed that β-carotene and retinoic acid regulate lipid transfer to the embryo by modulating MTTP expression and activity in placental tissue. However, they showed that this mechanism does not operate in the liver, in agreement with our findings (supplemental Fig. S3). Another factor that may modulate VLDL secretion is apoC-III, which facilitates the assembly and secretion of VLDL in McA cells (60). A recent study shows that retinoic acid decreases *apoC-III* expression (61); however, we detected no significant impact upon retinoic acid exposure in either McA cells or mouse liver (supplemental Fig. S3). Cell-type-dependent differences could explain the lack of consistency between studies (61, 62).

Zolberg Relevy et al. (37) showed that BCO1 is expressed and active in cultured macrophages, where its activity on provitamin A carotenoids inhibited foam cell formation. The stimulatory effect of retinoids on cholesterol efflux may mediate these effects (63), which would indicate that macrophage-specific BCO1 expression contributes to the delay of atherosclerosis progression in our model (Fig. 2). To test this hypothesis, we performed bone marrow transplants using wild-type and *Bco1*<sup>-/-</sup> as donor mice and *Ldlr*<sup>-/-</sup>/*Bco1*<sup>-/-</sup> as recipient mice (Fig. 5). Our histological analyses showed that myeloid-specific ablation of BCO1 affects neither atherosclerosis development nor plasma lipid levels (Fig. 5, supplemental Fig. S2A, B). Our RNA sequencing data in plaque myeloid cells showed a decrease in *Cyp26a1* expression in BCO1-deficient plaque cells compared with wild-type cells (Fig. 5H). We observed these results in the presence of circulating β-carotene, which is the substrate of BCO1 and the precursor of vitamin A and retinoic acid (supplemental Fig. S2C) (52).


The downregulation of *Aldh1a2*, a rate-limiting enzyme of retinoic acid synthesis, could also explain the reduction of retinoic acid signaling in BCO1-deficient plaque cells (Fig. 5H). Interestingly, *Aldh1a2* is also an anti-inflammatory (M2) macrophage marker (64), and the correct macrophage response to various infectious models requires its

activity (65–67). Our RNA sequencing data are aligned with a decreased M2-like phenotype in BCO1-deficient plaque myeloid cells, as TGFβ signaling is upregulated during M2 macrophage polarization (68–70) (Fig. 5 I, J).

Based on our data, BCO1 expression in myeloid cells does not impact atherosclerosis progression in mice, even in the presence of systemic β-carotene. Our HPLC and gene expression analyses showing no differences between groups in systemic or hepatic β-carotene levels, hepatic vitamin A stores, or retinoic acid-responsive genes in the liver support this outcome (supplemental Fig. S2G). The low expression of BCO1 in myeloid cells may partially explain these results. For instance, the absolute expression of BCO1 in wild-type plaque myeloid cells was modest (supplemental Table S2), in agreement with our data utilizing bone marrow-derived macrophages in which we could not detect BCO1 expression by mRNA sequencing (data not shown).

In summary, our results provide mechanistic insight on our recent findings in mice and humans in which we showed that BCO1 activity modulates plasma cholesterol (10). This study provides evidence that the conversion of β-carotene to vitamin A regulates hepatic lipoprotein secretion and atherosclerosis development in mice. BCO1 activity, possibly in the liver, mediates these effects, and they are independent of myeloid-specific BCO1 and intestinal cholesterol uptake. Future studies will aim to determine the molecular mechanisms by which vitamin A modulates the lipid profile and its pathological consequences in human subjects beyond alterations of plasma cholesterol. Nevertheless, this study significantly extends the implication of β-carotene and vitamin A in the risk of developing ASCVD.

#### Data availability

The data described in this article are presented in the figures or supplemental material. The RNA sequencing data have been deposited to NCBI's Gene Expression Omnibus and are accessible through GEO Series accession number GSE157972. 



#### Acknowledgments

We thank Alireza Khodadadi-Jamayran for his help in analyzing the RNA sequencing data.

#### Author contributions

F.Z., X.W., I.P., B.M.A., and J.A. experiments; T.J.B., J.v.L., E.A.F., and J.A. experiment design; F.Z., X.W., I.P., and J.A. data analyses; I.P. and J.A. statistical analyses; J.A. writing-original draft; F.Z., X.W., I.P., B.M.A., T.J.B., J.v.L., E.A.F., and J.A. writing-review and editing.

#### Author ORCIDs

Johannes von Lintig  <https://orcid.org/0000-0002-2079-2143>; Jaume Amengual  <https://orcid.org/0000-0002-6077-3545>

#### Funding and additional information

This work was supported by American Heart Association Grants 18CDA34110203 (T.J.B.) and 16SDG27550012 (J.A.);

National Institutes of Health Grants R01 EY028121 (J.v.L.), R01 HL084312 (E.A.F.), R01 HL127930 (E.A.F.), and R01 HL147252 (J.A.); US Department of Agriculture Grant W4002 (J.A.); and American Society of Hematology Grant 18-A0-00-1001884 (T.J.B.). The contents of this article do not represent the views of the Department of Agriculture or the United States Government. The content is solely the responsibility of the authors and does not necessarily represent the official views of the National Institutes of Health.

#### Conflict of interest

The authors declare that they have no conflicts of interest with the contents of this article.

#### Abbreviations

ASCVD, atherosclerotic cardiovascular disease; BCO1,  $\beta$ -carotene oxygenase 1; *Isx*, intestine-specific homeobox; McA, McArdle RH-7777; OCT, optimal cutting temperature; ORO, Oil Red O; Sr-bI, scavenger receptor class B type I; VAD, vitamin A-deficient.

Manuscript received August 4, 2020, and in revised form September 16, 2020. Published, JLR Papers in Press, September 22, 2020, DOI 10.1194/jlr.RA120001066.

## REFERENCES

- Mitchell, D. C., M. R. Prince, J. K. Frisoli, R. E. Smith, and R. F. Wood. 1993. Beta carotene uptake into atherosclerotic plaque: enhanced staining and preferential ablation with the pulsed dye laser. *Lasers Surg. Med.* **13**: 149–157.
- Christensen, K., T. Lawler, and J. Mares. 2019. Dietary carotenoids and non-alcoholic fatty liver disease among US Adults, NHANES 2003–2014. *Nutrients*. **11**: 1101.
- Huang, J., S. J. Weinstein, K. Yu, S. Mannisto, and D. Albanes. 2018. Serum beta carotene and overall and cause-specific mortality. *Circ. Res.* **123**: 1339–1349.
- Beydoun, M. A., X. Chen, K. Jha, H. A. Beydoun, A. B. Zonderman, and J. A. Canas. 2019. Carotenoids, vitamin A, and their association with the metabolic syndrome: a systematic review and meta-analysis. *Nutr. Rev.* **77**: 32–45.
- Bonet, M. L., J. Ribot, S. Galmes, F. Serra, and A. Palou. 2020. Carotenoids and carotenoid conversion products in adipose tissue biology and obesity: pre-clinical and human studies. *Biochim. Biophys. Acta Mol. Cell Biol. Lipids*. **1865**: 158676.
- Clugston, R. D. 2020. Carotenoids and fatty liver disease: current knowledge and research gaps. *Biochim. Biophys. Acta Mol. Cell Biol. Lipids*. **1865**: 158597.
- Miller, A. P., J. Coronel, and J. Amengual. 2020. The role of beta-carotene and vitamin A in atherogenesis: evidences from preclinical and clinical studies. *Biochim. Biophys. Acta Mol. Cell Biol. Lipids*. **1865**: 158635.
- von Lintig, J., and K. Vogt. 2000. Filling the gap in vitamin A research. Molecular identification of an enzyme cleaving beta-carotene to retinal. *J. Biol. Chem.* **275**: 11915–11920.
- Hessel, S., A. Eichinger, A. Isken, J. Amengual, S. Hunzelmann, U. Hoeller, V. Elste, W. Hunziker, R. Goralczyk, V. Oberhauser, et al. 2007. CMO1 deficiency abolishes vitamin A production from beta-carotene and alters lipid metabolism in mice. *J. Biol. Chem.* **282**: 33553–33561.
- Amengual, J., J. Coronel, C. Marques, C. Aradillas-Garcia, J. M. V. Morales, F. C. D. Andrade, J. W. Erdman, and M. Teran-Garcia. 2020. Beta-carotene oxygenase 1 activity modulates circulating cholesterol concentrations in mice and humans. *J. Nutr.* **150**: 2023–2030.
- Amengual, J., M. Golczak, K. Palczewski, and J. von Lintig. 2012. Lecithin:retinol acyltransferase is critical for cellular uptake of vitamin A from serum retinol-binding protein. *J. Biol. Chem.* **287**: 24216–24227.

- Amengual, J., G. P. Lobo, M. Golczak, H. N. Li, T. Klimova, C. L. Hoppel, A. Wyss, K. Palczewski, and J. von Lintig. 2011. A mitochondrial enzyme degrades carotenoids and protects against oxidative stress. *FASEB J.* **25**: 948–959.
- Amengual, J., N. Zhang, M. Kemerer, T. Maeda, K. Palczewski, and J. Von Lintig. 2014. STRA6 is critical for cellular vitamin A uptake and homeostasis. *Hum. Mol. Genet.* **23**: 5402–5417.
- Schindelin, J., I. Arganda-Carreras, E. Frise, V. Kaynig, M. Longair, T. Pietzsch, S. Preibisch, C. Rueden, S. Saalfeld, B. Schmid, et al. 2012. Fiji: an open-source platform for biological-image analysis. *Nat. Methods*. **9**: 676–682.
- Dole, V. P. 1956. A relation between non-esterified fatty acids in plasma and the metabolism of glucose. *J. Clin. Invest.* **35**: 150–154.
- Amengual, J., L. Guo, A. Strong, J. Madrigal-Matute, H. Wang, S. Kaushik, J. L. Brodsky, D. J. Rader, A. M. Cuervo, E. A. Fisher. 2018. Autophagy is required for sortilin-mediated degradation of apolipoprotein B100. *Circ. Res.* **122**: 568–582.
- Felipe, F., M. L. Bonet, J. Ribot, and A. Palou. 2004. Modulation of resistin expression by retinoic acid and vitamin A status. *Diabetes*. **53**: 882–889.
- Berry, D. C., and N. Noy. 2009. All-trans-retinoic acid represses obesity and insulin resistance by activating both peroxisome proliferation-activated receptor beta/delta and retinoic acid receptor. *Mol. Cell. Biol.* **29**: 3286–3296.
- Gerber, L. E., and J. W. Erdman, Jr. 1980. Comparative effects of all-trans and 13-cis retinoic acid administration on serum and liver lipids in rats. *J. Nutr.* **110**: 343–351.
- Krupková, M., M. Janku, F. Liska, L. Sedova, L. Kazdova, D. Krenova, V. Kren, O. Seda. 2009. Pharmacogenetic model of retinoic acid-induced dyslipidemia and insulin resistance. *Pharmacogenomics*. **10**: 1915–1927.
- Yu, M., J. Amengual, A. Menon, N. Kamaly, F. Zhou, X. Xu, P. E. Saw, S.-J. Lee, K. Si, C. A. Ortega, et al. 2017. Targeted nanotherapeutics encapsulating liver X receptor agonist GW3965 enhance antiatherogenic effects without adverse effects on hepatic lipid metabolism in *Ldlr*( $-/-$ ) mice. *Adv. Healthc. Mater.* **6**: 10.1002/adhm.201700313.
- Josefs, T., T. J. Barrett, E. J. Brown, A. Quezada, X. Wu, M. Voisin, J. Amengual, and E. A. Fisher. 2020. Neutrophil extracellular traps promote macrophage inflammation and impair atherosclerosis resolution in diabetic mice. *JCI Insight*. **5**: e134796.
- Dobin, A., C. A. Davis, F. Schlesinger, J. Drenkow, C. Zaleski, S. Jha, P. Batut, M. Chaisson, and T. R. Gingeras. 2013. STAR: ultrafast universal RNA-seq aligner. *Bioinformatics*. **29**: 15–21.
- Anders, S., P. T. Pyl, and W. Huber. 2015. HTSeq—a Python framework to work with high-throughput sequencing data. *Bioinformatics*. **31**: 166–169.
- Love, M. I., W. Huber, and S. Anders. 2014. Moderated estimation of fold change and dispersion for RNA-seq data with DESeq2. *Genome Biol.* **15**: 550.
- Quinlan, A. R., and I. M. Hall. 2010. BEDTools: a flexible suite of utilities for comparing genomic features. *Bioinformatics*. **26**: 841–842.
- Wang, D. Q., and M. C. Carey. 2003. Measurement of intestinal cholesterol absorption by plasma and fecal dual-isotope ratio, mass balance, and lymph fistula methods in the mouse: an analysis of direct versus indirect methodologies. *J. Lipid Res.* **44**: 1042–1059.
- Blaner, W. S., Y. Li, P. J. Brun, J. J. Yuen, S. A. Lee, R. D. Clugston, and A. Vitamin. 2016. Absorption, storage and mobilization. *Subcell. Biochem.* **81**: 95–125.
- Abu-Abed, S., P. Dolle, D. Metzger, B. Beckett, P. Chambon, and M. Petkovich. 2001. The retinoic acid-metabolizing enzyme, CYP26A1, is essential for normal hindbrain patterning, vertebral identity, and development of posterior structures. *Genes Dev.* **15**: 226–240.
- Stary, H. C., A. B. Chandler, R. E. Dinsmore, V. Fuster, S. Glagov, W. Insull, Jr., M. E. Rosenfeld, C. J. Schwartz, W. D. Wagner, and R. W. Wissler. 1995. A definition of advanced types of atherosclerotic lesions and a histological classification of atherosclerosis. A report from the Committee on Vascular Lesions of the Council on Arteriosclerosis, American Heart Association. *Circulation*. **92**: 1355–1374.
- Widjaja-Adhi, M. A., G. P. Lobo, M. Golczak, and J. Von Lintig. 2015. A genetic dissection of intestinal fat-soluble vitamin and carotenoid absorption. *Hum. Mol. Genet.* **24**: 3206–3219.
- Seino, Y., T. Miki, H. Kiyonari, T. Abe, W. Fujimoto, K. Kimura, A. Takeuchi, Y. Takahashi, Y. Oiso, T. Iwanaga, et al. 2008. *Isx* participates in the maintenance of vitamin A metabolism by regulation of

- beta-carotene 15,15'-monooxygenase (Bcmo1) expression. *J. Biol. Chem.* **283**: 4905–4911.
33. Kiefer, C., E. Sumser, M. F. Wernet, and J. Von Lintig. 2002. A class B scavenger receptor mediates the cellular uptake of carotenoids in *Drosophila*. *Proc. Natl. Acad. Sci. USA.* **99**: 10581–10586.
  34. Shen, W. J., S. Azhar, and F. B. S. R. Kraemer. 2018. SR-BI: a unique multifunctional receptor for cholesterol influx and efflux. *Annu. Rev. Physiol.* **80**: 95–116.
  35. Meex, S. J., U. Andreo, J. D. Sparks, and E. A. Fisher. 2011. Huh-7 or HepG2 cells: which is the better model for studying human apolipoprotein-B100 assembly and secretion? *J. Lipid Res.* **52**: 152–158.
  36. Feingold, K. R., and C. Grunfeld. 2000. Introduction to lipids and lipoproteins. In *Endotext*. K. R. Feingold, B. Anawalt, A. Boyce, et al., editors. MDText.com, Inc., South Dartmouth, MA.
  37. Zolberg Relevy, N., S. Bechor, A. Harari, A. Ben-Amotz, Y. Kamari, D. Harats, and A. Shaish. 2015. The inhibition of macrophage foam cell formation by 9-cis beta-carotene is driven by BCMO1 activity. *PLoS One.* **10**: e0115272.
  38. Niederreither, K., V. Subbarayan, P. Dolle, and P. Chambon. 1999. Embryonic retinoic acid synthesis is essential for early mouse post-implantation development. *Nat. Genet.* **21**: 444–448.
  39. Cai, K., and L. J. Gudas. 2009. Retinoic acid receptors and GATA transcription factors activate the transcription of the human lecithin:retinol acyltransferase gene. *Int. J. Biochem. Cell Biol.* **41**: 546–553.
  40. Leung, W. C., S. Hessel, C. Meplan, J. Flint, V. Oberhauser, F. Tourniaire, J. E. Hesketh, J. von Lintig, and G. Lietz. 2009. Two common single nucleotide polymorphisms in the gene encoding beta-carotene 15,15'-monooxygenase alter beta-carotene metabolism in female volunteers. *FASEB J.* **23**: 1041–1053.
  41. Dixon, J. L., Y. K. Kim, A. Brinker, and L. Quadro. 2014. Loss of beta-carotene 15,15'-oxygenase in developing mouse tissues alters esterification of retinol, cholesterol and diacylglycerols. *Biochim. Biophys. Acta.* **1841**: 34–43.
  42. Lee, S. A., H. Jiang, C. M. Trent, J. J. Yuen, S. Narayanasamy, R. W. Curley, Jr., E. H. Harrison, I. J. Goldberg, M. S. Maurer, and W. S. Blaner. 2014. Cardiac dysfunction in beta-carotene-15,15'-dioxygenase-deficient mice is associated with altered retinoid and lipid metabolism. *Am. J. Physiol. Heart Circ. Physiol.* **307**: H1675–H1684.
  43. Amengual, J., E. Gouranton, Y. G. van Helden, S. Hessel, J. Ribot, E. Kramer, B. Kiec-Wilk, U. Razny, G. Lietz, A. Wyss, et al. 2011. Beta-carotene reduces body adiposity of mice via BCMO1. *PLoS One.* **6**: e20644.
  44. Harari, A., D. Harats, D. Marko, H. Cohen, I. Barshack, Y. Kamari, A. Gonen, Y. Gerber, A. Ben-Amotz, and A. Shaish. 2008. A 9-cis beta-carotene-enriched diet inhibits atherogenesis and fatty liver formation in LDL receptor knockout mice. *J. Nutr.* **138**: 1923–1930.
  45. Relevy, N. Z., D. Harats, A. Harari, A. Ben-Amotz, R. Bitzur, R. Ruhl, and A. Shaish. 2015. Vitamin A-deficient diet accelerated atherogenesis in apolipoprotein E(−/−) mice and dietary beta-carotene prevents this consequence. *BioMed Res. Int.* **2015**: 758723.
  46. Reeves, P. G., F. H. Nielsen, and G. C. Fahey, Jr. 1993. AIN-93 purified diets for laboratory rodents: final report of the American Institute of Nutrition ad hoc writing committee on the reformulation of the AIN-76A rodent diet. *J. Nutr.* **123**: 1939–1951.
  47. Ishibashi, S., M. S. Brown, J. L. Goldstein, R. D. Gerard, R. E. Hammer, and J. Herz. 1993. Hypercholesterolemia in low density lipoprotein receptor knockout mice and its reversal by adenovirus-mediated gene delivery. *J. Clin. Invest.* **92**: 883–893.
  48. Carson, J. A. S., A. H. Lichtenstein, C. A. M. Anderson, L. J. Appel, P. M. Kris-Etherton, K. A. Meyer, K. Petersen, T. Polonsky, L. Van Horn, American Heart Association Nutrition Committee of the Council on Lifestyle and Cardiometabolic Health, et al. 2020. Dietary cholesterol and cardiovascular risk: a science advisory from the American Heart Association. *Circulation.* **141**: e39–e53.
  49. Lobo, G. P., J. Amengual, D. Baus, R. A. Shivdasani, D. Taylor, and J. von Lintig. 2013. Genetics and diet regulate vitamin A production via the homeobox transcription factor ISX. *J. Biol. Chem.* **288**: 9017–9027.
  50. Bura, K. S., C. Lord, S. Marshall, A. McDaniel, G. Thomas, M. Warrior, J. Zhang, M. A. Davis, J. K. Sawyer, R. Shah, et al. 2013. Intestinal SR-BI does not impact cholesterol absorption or transintestinal cholesterol efflux in mice. *J. Lipid Res.* **54**: 1567–1577.
  51. Fisher, E. A. 2012. The degradation of apolipoprotein B100: multiple opportunities to regulate VLDL triglyceride production by different proteolytic pathways. *Biochim. Biophys. Acta.* **1821**: 778–781.
  52. Coronel, J., I. Pinos, and J. Amengual. 2019.  $\beta$ -Carotene in obesity research: technical considerations and current status of the field. *Nutrients.* **11**: 842.
  53. Amengual, J., J. Ribot, M. L. Bonet, and A. Palou. 2008. Retinoic acid treatment increases lipid oxidation capacity in skeletal muscle of mice. *Obesity (Silver Spring).* **16**: 585–591.
  54. Amengual, J., J. Ribot, M. L. Bonet, and A. Palou. 2010. Retinoic acid treatment enhances lipid oxidation and inhibits lipid biosynthesis capacities in the liver of mice. *Cell. Physiol. Biochem.* **25**: 657–666.
  55. Amengual, J., P. Petrov, M. L. Bonet, J. Ribot, and A. Palou. 2012. Induction of carnitine palmitoyl transferase 1 and fatty acid oxidation by retinoic acid in HepG2 cells. *Int. J. Biochem. Cell Biol.* **44**: 2019–2027.
  56. Amengual, J., F. J. Garcia-Carrizo, A. Arreguin, H. Musinovic, N. Granados, A. Palou, M. L. Bonet, and J. Ribot. 2018. Retinoic acid increases fatty acid oxidation and irisin expression in skeletal muscle cells and impacts irisin in vivo. *Cell. Physiol. Biochem.* **46**: 187–202.
  57. Mercader, J., L. Madsen, F. Felipe, A. Palou, K. Kristiansen, and M. L. Bonet. 2007. All-trans retinoic acid increases oxidative metabolism in mature adipocytes. *Cell. Physiol. Biochem.* **20**: 1061–1072.
  58. Hussain, M. M., P. Rava, M. Walsh, M. Rana, and J. Iqbal. 2012. Multiple functions of microsomal triglyceride transfer protein. *Nutr. Metab. (Lond.)* **9**: 14.
  59. Costabile, B. K., Y. K. Kim, J. Iqbal, M. V. Zuccaro, L. Wassef, S. Narayanasamy, R. W. Curley, Jr., E. H. Harrison, M. M. Hussain, and L. Quadro. 2016.  $\beta$ -Apo-10'-carotenoids modulate placental microsomal triglyceride transfer protein expression and function to optimize transport of intact beta-carotene to the embryo. *J. Biol. Chem.* **291**: 18525–18535.
  60. Sundaram, M., S. Zhong, M. Bou Khalil, P. H. Links, Y. Zhao, J. Iqbal, M. M. Hussain, R. J. Parks, Y. Wang, and Z. Yao. 2010. Expression of apolipoprotein C-III in McA-RH7777 cells enhances VLDL assembly and secretion under lipid-rich conditions. *J. Lipid Res.* **51**: 150–161.
  61. Lee, S. J., M. Mahankali, A. Bitar, H. Zou, E. Chao, H. Nguyen, J. Gonzalez, D. Caballero, M. Hull, D. Wang, et al. 2017. A novel role for RAR $\alpha$  agonists as apolipoprotein CIII inhibitors identified from high throughput screening. *Sci. Rep.* **7**: 5824.
  62. Howell, M., R. Li, R. Zhang, Y. Li, W. Chen, and G. Chen. 2014. The expression of Apoc3 mRNA is regulated by HNF4 $\alpha$  and COUP-TFII, but not acute retinoid treatments, in primary rat hepatocytes and hepatoma cells. *Mol. Cell. Biochem.* **387**: 241–250.
  63. Costet, P., F. Lalanne, M. C. Gerbod-Giannone, J. R. Molina, X. Fu, E. G. Lund, L. J. Gudas, and A. R. Tall. 2003. Retinoic acid receptor-mediated induction of ABCA1 in macrophages. *Mol. Cell. Biol.* **23**: 7756–7766.
  64. Broadhurst, M. J., J. M. Leung, K. C. Lim, N. M. Girgis, U. M. Gundra, P. G. Fallon, M. Premenko-Lanier, J. H. McKerrow, J. M. McCune, and P. Loke. 2012. Upregulation of retinal dehydrogenase 2 in alternatively activated macrophages during retinoid-dependent type-2 immunity to helminth infection in mice. *PLoS Pathog.* **8**: e1002883.
  65. Girgis, N. M., U. M. Gundra, L. N. Ward, M. Cabrera, U. Frevert, and P. Loke. 2014. Ly6Chigh monocytes become alternatively activated macrophages in schistosome granulomas with help from CD4+ cells. *PLoS Pathog.* **10**: e1004080.
  66. Gundra, U. M., N. M. Girgis, D. Ruckerl, S. Jenkins, L. N. Ward, Z. D. Kurtz, K. E. Wiens, M. S. Tang, U. Basu-Roy, A. Mansukhani, et al. 2014. Alternatively activated macrophages derived from monocytes and tissue macrophages are phenotypically and functionally distinct. *Blood.* **123**: e110–e122.
  67. Gundra, U. M., N. M. Girgis, M. A. Gonzalez, M. San Tang, H. J. P. Van Der Zande, J. D. Lin, M. Ouimet, L. J. Ma, J. Poles, N. Vozhilla, et al. 2017. Vitamin A mediates conversion of monocyte-derived macrophages into tissue-resident macrophages during alternative activation. *Nat. Immunol.* **18**: 642–653.
  68. Zhang, F., H. Wang, X. Wang, G. Jiang, H. Liu, G. Zhang, H. Wang, R. Fang, X. Bu, S. Cai, et al. 2016. TGF-beta induces M2-like macrophage polarization via SNAIL-mediated suppression of a pro-inflammatory phenotype. *Oncotarget.* **7**: 52294–52306.
  69. Zhang, Y. H., M. He, Y. Wang, and A. H. Liao. 2017. Modulators of the balance between M1 and M2 macrophages during pregnancy. *Front. Immunol.* **8**: 120.
  70. Gong, D., W. Shi, S. J. Yi, H. Chen, J. Groffen, and N. Heisterkamp. 2012. TGFbeta signaling plays a critical role in promoting alternative macrophage activation. *BMC Immunol.* **13**: 31.